Jpn. J. Appl. Phys. Vol. 38 (1999) pp. 3716–3722
Part 1, No. 6A, June 1999

Characteristics of RF Wave Propagation in Large-Diameter Plasma with Cusp Magnetic Field Configurations

Seiji TAKECHI*[1], Shunjiro SHINOHARA*[2] and Atsushi FUKUYAMA[1]

Interdisciplinary Graduate School of Engineering Sciences, Kyushu University, Kasuga, Fukuoka 816-8580, Japan
[1] *Department of Nuclear Engineering, Faculty of Engineering, Kyoto University, Sakyo-ku, Kyoto 606-8501, Japan*

(Received November 24, 1998; accepted for publication March 11, 1999)

RF wave propagation, in the large-diameter (45 cm) plasma produced by a planar, spiral antenna, was investigated with the cusp magnetic field configurations. Measurements of the excited magnetic field amplitude and the phase were examined by a helicon wave dispersion relation, and the obtained results were consistent with the calculated ones by Transport Analyzing System for tokamaK/Wave analysis by Finite element method (TASK/WF) code. The wave characteristics depended on the gradient and the magnitude of the magnetic field near the line cusp position, and in the neighborhood of this position, this wave showed different behavior from the helicon wave observed in a uniform field.

KEYWORDS: RF plasma, spiral antenna, cusp magnetic field, helicon wave, numerical computation

1. Introduction

High-density plasma sources are becoming increasingly important for plasma processing and confinement devices. One promising souce is a helicon wave plasma[1–3] or inductively coupled plasma/transformer coupled plasma (ICP/TCP).[4] Both of them are produced by RF waves with and without the external magnetic field, respectively, and have been actively investigated theoretically and experimentally. In addition, a planar spiral coil[5,6] has been used in ICP because of the advantage of the relatively simple geometry.

In previous work,[6–8] in order to easily produce a plasma with better uniformity in the radial direction and high plasma density by ICP with the spiral antenna, we used various external magnetic field configurations under the relatively low field. With the uniform field, we could control the plasma density smoothly from low to high values, and the axial profile appeared flatter, but the radial profile of the electron density became more peaked. In addition, excitation of the helicon wave with an azimuthal mode number of $m = 0$ was demonstrated in large-diameter RF plasma using this type of antenna.[6,7] With the cusp field (< 50 G), the uniformity improved significantly[8] (effective diameter of 27 cm, which defines a region where ion saturation current was within $\pm 5\%$, with the plasma density of $\sim 10^{12}$ cm^{-3}) compared to the ICP case.

From these results, there may be a close relation between the density profile and regions of the wave propagation and damping. Therefore, analyzing the wave characteristics in the various field configurations as a control parameter is important for producing the desired plasma profiles, and can also provide interesting helicon wave physics, not with the uniform magnetic field configuration but with a nonuniform one, which has been scarcely investigated. Under limited conditions, the wave phenomena were investigated, changing the line cusp position as well as the gradient and magnitude of the magnetic field.[9,10]

In this work, we characterize the RF wave propagation under the various cusp magnetic field configurations by measuring the two-dimensional spatial profiles of the amplitude and the phase of the excited magnetic fields in the large-diameter plasma. The obtained results were examined by the helicon wave dispersion relation, and were compared to the computation results by the use of Transport Analyzing System for tokamaK/Wave analysis by Finite element method (TASK/WF) code developed by one of our authors (A.F.).

2. Experimental Setup

The experimental system is shown in Fig. 1 The four-turn, water-cooled, spiral antenna of 18 cm diameter was made of copper. The distance between the surface of the antenna and the quartz window, which was 25 cm in diameter and 0.8 cm thick, was 1.7 cm. Here, $z = 0$ cm was defined as being at the window surface which faces an inner vacuum chamber, ~ 45 cm in diameter and 170 cm in length. The applied cusp magnetic field was generated by only two coils: currents with the same magnitude had opposite directions. In this study, the line cusp position was fixed at $z = 30$ cm and the central distance d between the two coils (48 turns each), which reflected the gradient scale length L of the cusp magnetic field, was varied. Here, L was defined as the distance between the cusp position and the cross point of two tangents, taken at the cusp position and at the position having the maximum magnitude value of the magnetic field. Axial profiles of the absolute value of the magnetic field B for three typical cases are shown in Fig. 2: (a) $d = 88$ cm and the coil current $I_c = 60$ A, (b) $d = 42$ cm and $I_c = 60$ A and (c) $d = 16$ cm and $I_c = 120$ A.

In our experiments, RF input power was $\sim$ 300 W with

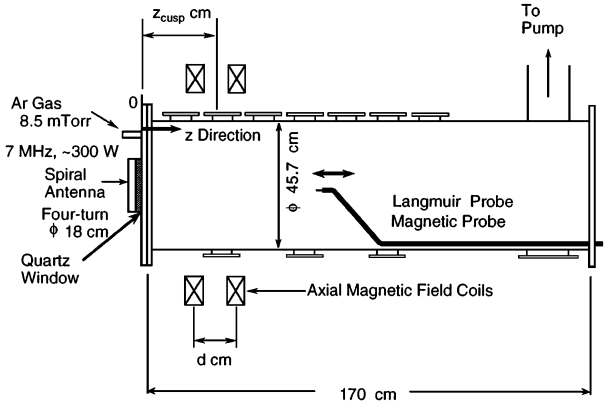

Fig. 1. Schematic view of experimental device.

*[1]E-mail: takechi@aees.kyushu-u.ac.jp
*[2]E-mail: sinohara@aees.kyushu-u.ac.jp

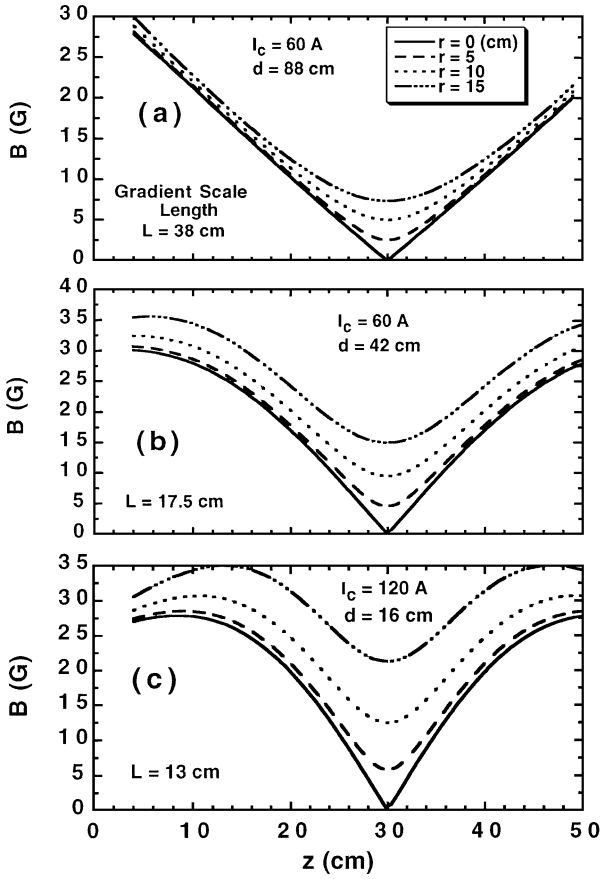

Fig. 2. Axial profiles of the magnitude of the external magnetic field with (a) d (central distance between two coils) = 88 cm and I_c (coil current) = 60 A, (b) d = 42 cm and I_c = 60 A and (c) d = 16 cm and I_c = 120 A.

a frequency ($\omega/2\pi$) of 7 MHz and Ar filling pressure of 8.5 mTorr. Ar plasma parameters were measured by the use of movable and rotatable Langmuir (1 mm in diameter with 3 mm length) and magnetic (one-turn coil with 7 mm in diameter) probes inserted axially into the plasma (main measuring region was z = 3–50 cm with four radial positions of r = 0, 5, 10 and 15 cm). Typical electron temperature T_e was 2–3 eV, and the electron density n_e near the antenna was $< 10^{12}$ cm^{-3}.

3. Experimental Results

Figure 3 (4) shows two-dimensional contour plots of the amplitude (phase) of the radial, azimuthal and axial components of the excited magnetic field, (a) B_r, (b) B_θ and (c) B_z, respectively, in logarithmic (linear) scale, for the case of d = 88 cm and I_c = 60 A. The intervals between the contour lines in Figs. 3 and 4 were 0.2 and $\pi/2$, respectively. It can be seen that the amplitudes of B_r and B_θ was larger at off axis, while that of B_z was larger on axis, and these phases at a fixed z position changed $\sim \pi$ radians in the radial direction from the central axis to the wall. Although the radial resolution of 5 cm was not good, these characteristics are the same as that of the helicon wave with an azimuthal mode number of m = 0 mode. It is also shown from Fig. 3 that the excited wave damped strongly near the cusp position of z = 30 cm. For the case of the weaker current of I_c = 30 A, the wave damped more strongly before the cusp position.

Figures 5(a) and 5(b) show the check of the dispersion relation for the m = 0 mode helicon wave with a fundamental

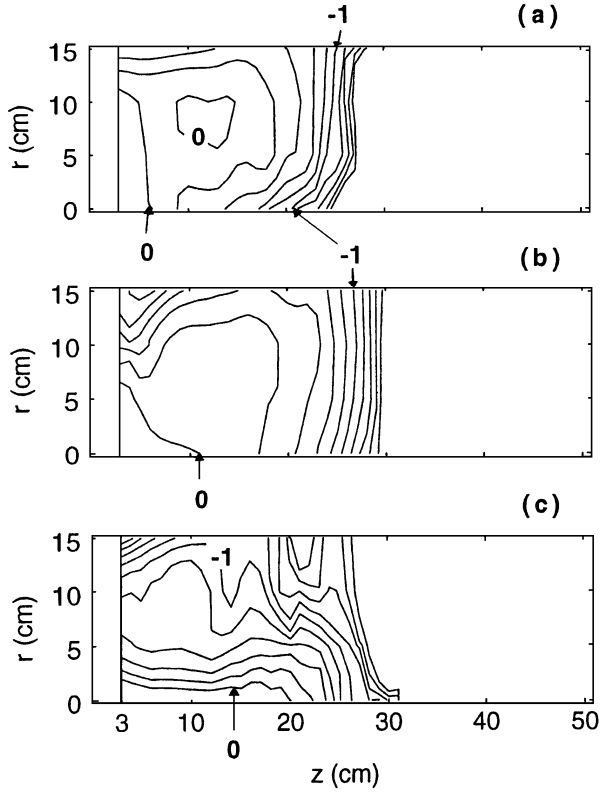

Fig. 3. Contour plots (logarithmic scale) of amplitude of (a) B_r, (b) B_θ and (c) B_z with d = 88 cm and I_c = 60 A.

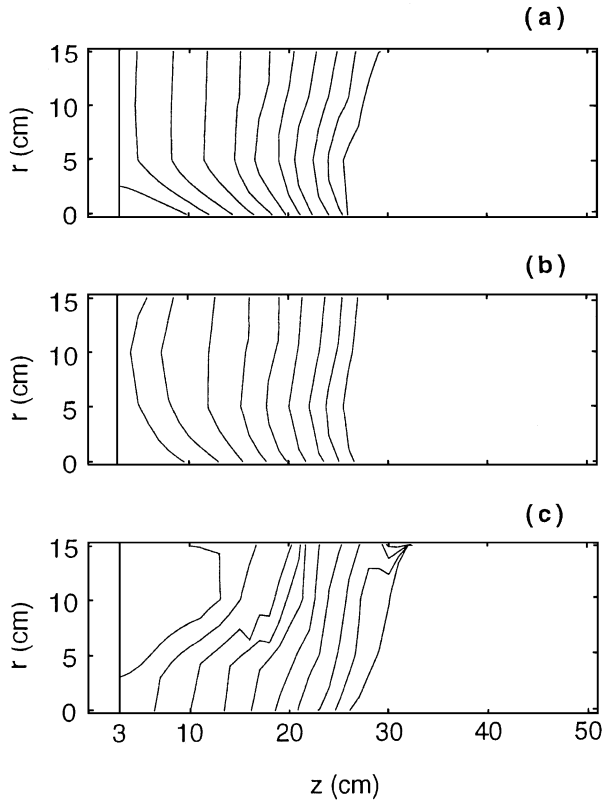

Fig. 4. Contour plots (linear scale) of phase of (a) B_r, (b) B_θ and (c) B_z with d = 88 cm and I_c = 60 A.

radial mode[2] for the case of d = 88 cm with I_c = 30 A and 60 A, respectively (ω_{pe}: electron plasma angular frequency, ω_{ce}: electron cyclotron angular frequency, c: velocity of

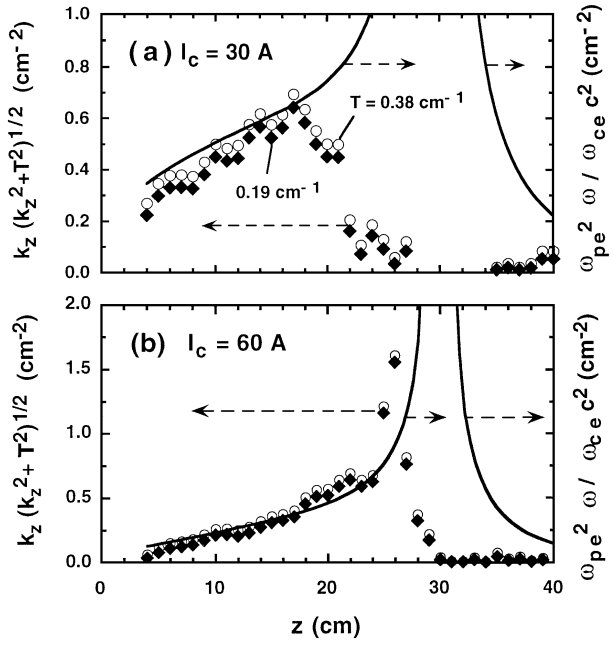

Fig. 5. Dispersion relation as a function of z for the case of $d = 88$ cm with (a) $I_c = 30$ A and (b) $I_c = 60$ A. Left vertical axis of $k_z(k_z^2 + T^2)^{0.5}$ is estimated with $T = 0.19\,\mathrm{cm}^{-1}$ (closed lozenges) and $0.38\,\mathrm{cm}^{-1}$ (open circles). Right vertical axis of $\omega_{pe}^2\omega/\omega_{ce}c^2$ is derived using magnitude of the magnetic field B and electron density n_e (solid lines).

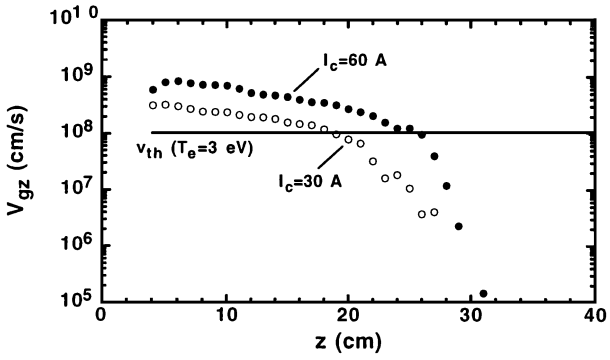

Fig. 6. Axial profiles of group velocity (z direction) V_{gz} on axis for the case of $d = 88$ cm with $I_c = 30$ A and 60 A. For comparison, the electron thermal velocity v_{th} with $T_e = 3$ eV is also shown.

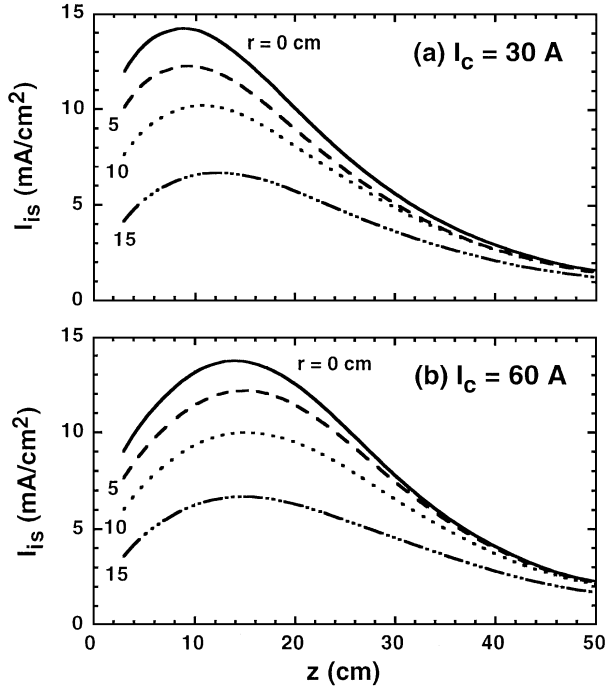

Fig. 7. Axial profiles of ion saturation current for the case of $d = 88$ cm with (a) $I_c = 30$ A and (b) $I_c = 60$ A.

light). Here, the parallel wave number k_z (along the z axis, irrespective of the direction of the magnetic field line) was determined by the axial profile of the excited magnetic field on axis with an assumption of the perpendicular wave number $T = 3.83/a$ to derive $k_z(k_z^2 + T^2)^{0.5}$ (left vertical axis). Here, the effective radii were taken as $a = 10$ cm and 20 cm for $T = 0.38$ and $0.19\,\mathrm{cm}^{-1}$, respectively. The measured n_e and calculated B were used to derive the curve (right vertical axis), since n_e/B is proportional to $k_z(k_z^2 + T^2)^{0.5}$. It is found that with increasing I_c, the region of agreement between the two estimations approaced the line cusp position, and near the cusp position at $B \sim 8$ G, the $k_z(k_z^2 + T^2)^{0.5}$ term decreased and deviated from the $\omega_{pe}^2\omega/\omega_{ce}c^2$ curve due to the bending of the magnetic field. This shows that the excited $m = 0$ mode helicon wave with a fundamental perpendicular wave number could propagate closer to the cusp position with increasing the magnetic field.

Figure 6 shows the axial component of the group velocity V_{gz} on axis, which was estimated from the formula in ref. 11, for the same case as of Fig. 5 with $d = 88$ cm. This shows that the V_{gz} value was larger with the higher I_c value, and the z-position with $V_{gz} = v_{th}$ (electron thermal velocity with $T_e = 3$ eV) approaced the cusp position. This tendency is consistent with the region of disagreement of the dispersion curve in Fig. 5. For the helicon wave with the uniform plasma density and magnetic field ($\omega \ll \omega_{ce}$), when $k_z \sim T$, which satisfied the present case, V_{gz} is nearly proportional to $B^{1.5}/n_e^{0.5}$. Note that this formula is the same as that for the case of $k_z \gg T$, while when $k_z \ll T$, V_{gz} is proportional to B/T. Therefore, V_{gz} is strongly dependent on the magnitude of the magnetic field B compared to the electron density. The above results from Figs. 5 and 6 can be considered as follows. For the helicon wave to propagate, it was necessary that the B value was above the critical value $B_c \sim 8$ G. This was also found in ref. 7, in which B_c was 10–20 G for the wave propagation from the antenna to $z = 30$ cm with the uniform field and RF power of $\sim$ 1.7 kW. We must consider the rapidly varying propagation medium (external magnetic field) over a wavelength.

Figure 7 shows the axial profiles of ion saturation current I_{is} for the above case of $d = 88$ cm with (a) $I_c = 30$ A and (b) $I_c = 60$ A, respectively. The position of the peak value shifted to the right (more positive z-position) with increasing I_c, i.e., increasing B. This result can be considered to be a reflection from the above results that the wave propagated more deeply to the z-position with increasing I_c.

The above results show that for the case of $d = 88$ cm ($L = 38$ cm), the $m = 0$ mode helicon wave propagated closer to the line cusp position with the larger field strength, but as it approached this position, the wave damped steeply.

Next, the wave characteristics were investigated with changing d, i.e., L. The two-dimensional contour plots of the amplitude of B_z are shown in Fig. 8 (see also Fig. 3 for

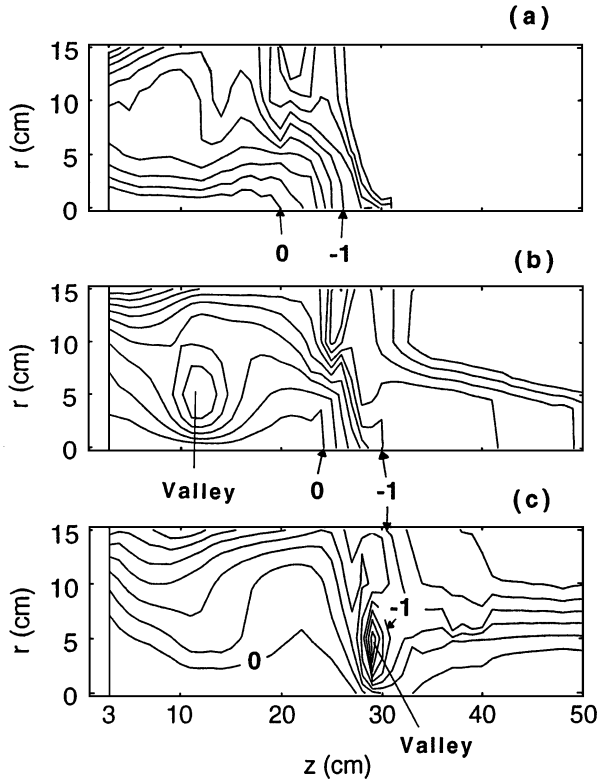

Fig. 8. Contour plots (logarithmic scale) of amplitude of B_z with (a) $d = 88$ cm and $I_c = 60$ A, (b) $d = 42$ cm and $I_c = 60$ A and (c) $d = 16$ cm and $I_c = 120$ A.

the case of Fig. 8(a) with $d = 88$ cm and $I_c = 60$ A). Figures 8(b) and 8(c) are shown for the case of $d = 42$ cm ($L = 17.5$ cm) with $I_c = 60$ A and $d = 16$ cm ($L = 13$ cm) with $I_c = 120$ A, respectively (the interval between contour lines was 0.2, which was the same as that in Fig. 3). Here, the maximum field strength for each field configuration was adjusted to be almost the same by choosing the I_c value (the maximum B was ~ 30 G from Fig. 2). The excited wave damped strongly near the cusp position for all the three cases, but as for the case of shorter d (L), the wave field could penetrate through the cusp position. For the case of Fig. 8(c), the wave amplitude decayed at the cusp and then increased beyond the cusp, which is clearly seen in the inner plasma region. For both cases of $d = 42$ cm (not shown) and $d = 16$ cm [see Fig. 10(d)], changes in the phase had the same tendency as that for $d = 88$ cm [Fig. 4(c)] before reaching the line cusp position, and beyond this position, the phase held almost constant for the case of $d = 42$ cm, while it increased slowly with z for the case of $d = 16$ cm. These results mean that the excited wave could propagate further beyond the cusp position when the gradient at the line cusp position became steeper with constant magnetic field strength, i.e., in the case of shorter L.

Figure 9 (10) shows two-dimensional contour plots of the amplitude (phase) of B_z for the case of $d = 16$ cm, changing the coil current: (a) $I_c = 30$ A, (b) $I_c = 60$ A, (c) $I_c = 90$ A and (d) $I_c = 120$ A. The scale and interval between contour lines in Figs. 9 and 10 were the same as those in Figs. 3 and 4, respectively. This shows that the excited wave could propagate beyond the line cusp position easier as the I_c value, i.e., the magnitude of the field B, was larger. Axial profiles

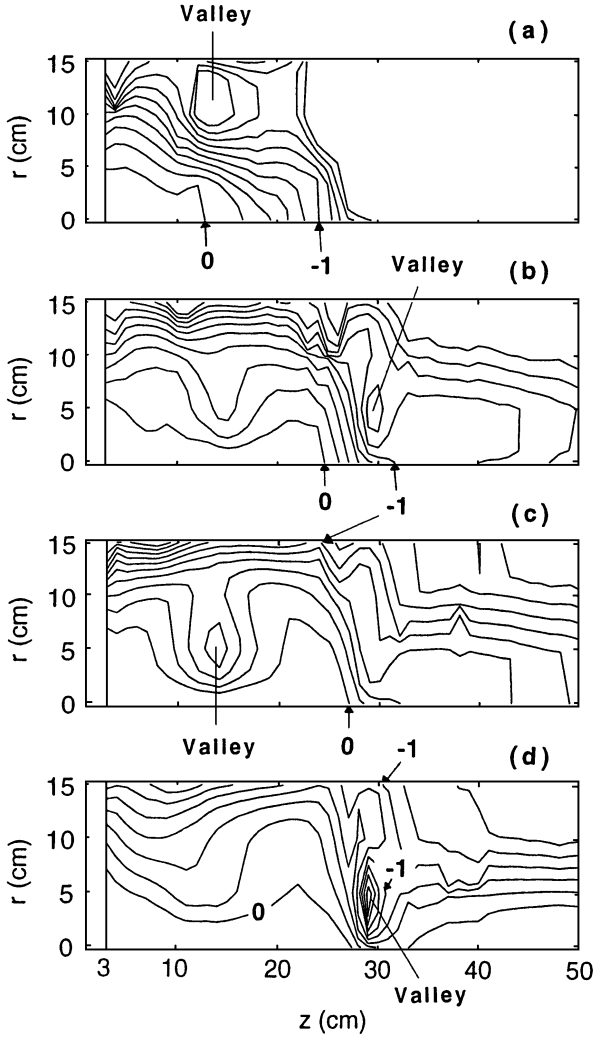

Fig. 9. Contour plots (logarithmic scale) of amplitude of B_z for the case of $d = 16$ cm with (a) $I_c = 30$ A, (b) $I_c = 60$ A, (c) $I_c = 90$ A and (d) $I_c = 120$ A.

of I_{is} reflected these wave phenomena in the neighborhood of the cusp position, i.e., nonmonotonic profile change at the off axis when the wave could propagate beyond the position.[10] This is consistent with the characteristics of the axial profile of V_{gz} (not shown) derived by the above-mentioned method. In addition, for the case of $d = 42$ cm, similar results were also obtained, and at $z \sim 45$ cm, the effective diameter, where the ion saturation current was within $\pm 5\%$, was ~ 30 cm with $I_c = 60$ A.[9] Examining the dispersion relation for both cases of $d = 42$ cm and $d = 16$ cm by the same method as that used in Fig. 5, there was a slight discrepancy before the line cusp position.[10] However, the phase change in the axial direction, depending on the magnitude of the magnetic field (*e.g.*, see Fig. 10 for the case of $d = 16$ cm), and the phase change in the radial direction, were consistent with the helicon wave dispersion relation with a fundamental radial mode. The large deviation from the helicon wave dispersion was roughly at the position of the critical field $B_c \sim 8$ G.

In summary, with the cusp magnetic field configuration, the excited wave damped strongly near the line cusp position (in the neighborhood of the critical value), and this wave could propagate further beyond this position when the magnetic field strength and/or the gradient of the field near the

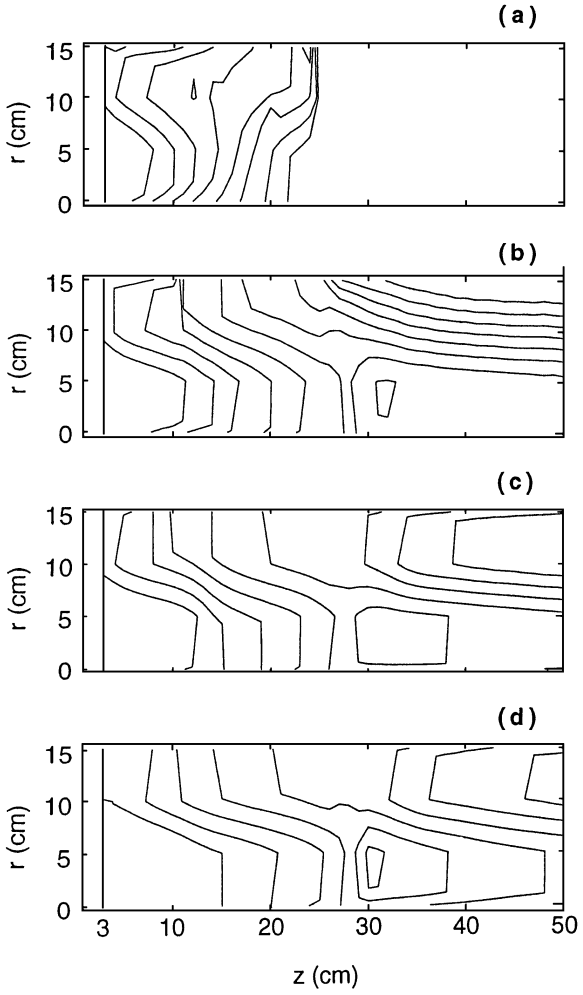

Fig. 10. Contour plots (linear scale) of phase of B_z for the case of $d = 16$ cm with (a) $I_c = 30$ A, (b) $I_c = 60$ A, (c) $I_c = 90$ A and (d) $I_c = 120$ A.

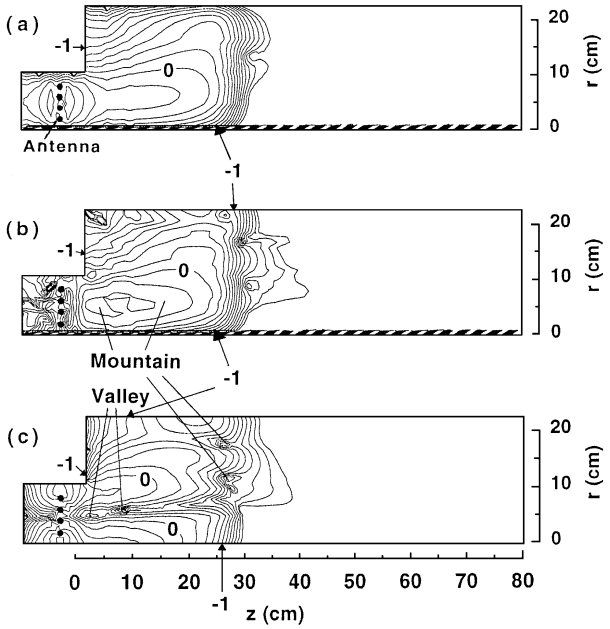

Fig. 11. Contour plots (logarithmic scale) of amplitude of (a) B_r, (b) B_θ and (c) B_z with $d = 88$ cm and $I_c = 60$ A (computation).

cusp position was larger. The dominant wave can be considered as the $m = 0$ mode helicon wave with a fundamental radial mode for the case of the longer d. For the shorter d case, the excited wave was not the conventional helicon wave, especially beyond the cusp position. This will be discussed via a comparison with the computation results in the next section.

4. Discussion with Computation Results

The TASK/WF code[12] was developed by Fukuyama, using the finite element method to solve vector and scalar potentials of the wave. This code analyzes wave propagation in an inhomogeneous medium (two and three dimensions) under various external magnetic field configurations, plasma density profiles, antenna geometries and boundary shapes. The response of a plasma is described by a cold-plasma dielectric tensor including collisions with neutrals. By use of this code, the helicon wave characteristics under the cusp field configurations obtained in the experiment can be understood in more detail.

First, the reliability of this code (here, the mesh interval was 1 cm in both the radial and axial directions) was confirmed by comparing with the following experimental results: I) Using the axial profile of the electron density observed for the case of $d = 88$ cm with $I_c = 60$ A; the results, i.e., two-dimensional contour plots of the RF wave amplitude of B_r, B_θ and B_z, are shown in Figs. 11(a), 11(b) and 11(c), respectively, in logarithmic scale (the interval between contour lines in Figs. 11(a)–11(c) was again the same as that in Fig 3). Here, the spiral antenna position is represented by filled circles in the left side of figures. Note that the spatial resolution in the radial direction (5 cm) is not good for the experiment, compared to the computation (1 cm), and thick shaded regions contain many contour lines in Figs. 11(a) and 11(b) because of approaching the zero value near the axis. It is found that the computation results, also including the phase plot (not shown), demonstrate the characteristic of the $m = 0$ mode helicon wave before the cusp position, whose characteristics were similar to the experimental ones in Figs. 3 and 4.

II) The axial profiles of B_z on axis for the case of $d = 16$ cm with $I_c = 120$ A obtained from the experiment and the computation using the experimentally obtained density profile, are shown in Figs. 12(a) and 12(b), respectively. Here, the real component, the imaginary component and the absolute value of the B_z are presented simultaneously. Both results agree well and show that the wavelength of the excited wave becomes longer by a factor of ~ 2 after passing through the line cusp position.

From both cases I) and II), in addition to the case of a uniform magnetic configuration, the computation results support the experimental ones. Therefore, it was confirmed that the wave did not interfere with the reflected wave but damped near the line cusp position, and could propagate beyond the line cusp position, depending on the magnetic field strength and/or the gradient of the field near the cusp position. We also found that the dominant mechanism of the steep wave damping near the position was not due to the effect of the electron thermal motion, because of the adopting the cold plasma approximation in the computation. Note that in ICP without any external magnetic field, the phase changed suddenly and the wave amplitude decayed near v_{ph} (phase velocity) $\sim v_{th}$ suggesting the effect of the finite electron temperature.[13]

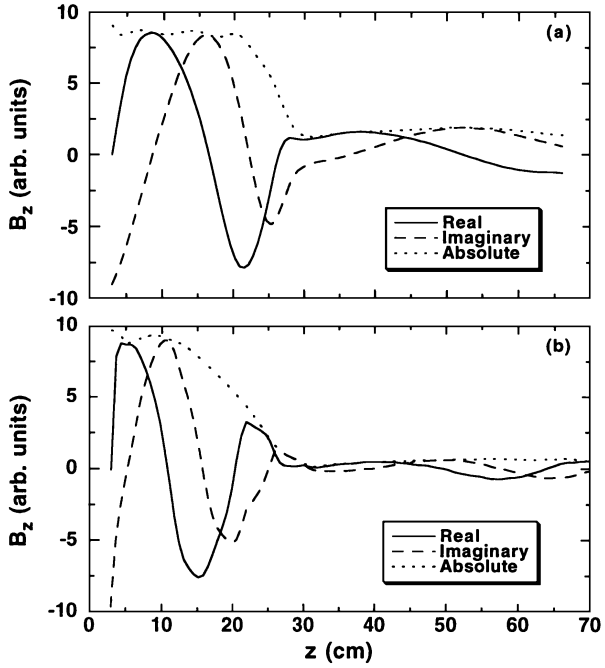

Fig. 12. Axial profiles of B_z on axis with $d = 16\,\mathrm{cm}$ and $I_c = 120\,\mathrm{A}$ from (a) experiment and (b) computation.

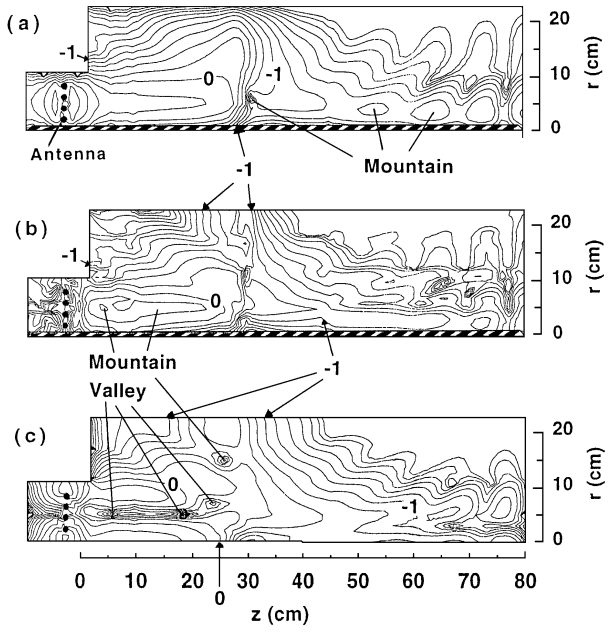

Fig. 13. Contour plots (logarithmic scale) of amplitude of (a) B_r, (b) B_θ and (c) B_z with $d = 16\,\mathrm{cm}$ and $I_c = 120\,\mathrm{A}$ (computation).

Here, we will consider the wave behavior in the neighborhood of the line cusp position. From Fig. 11 (computation), while approaching the line cusp position, the wave amplitude having a peaked profile broadened, because the wave at the off-axis region could penetrate beyond the cusp position compared to the one at the center axis, owing to the relatively higher magnetic field (absolute value is low). Figure 13 shows similar computation results of the three components of the excited magnetic fields for the case of $d = 16\,\mathrm{cm}$ with $I_c = 120\,\mathrm{A}$. From this figure, the excited wave region broadened before the cusp position and damped near this position, and after that, the amplitude of which the wave penetrated beyond the cusp converged towards the central axis along the field lines. In order to check the power deposition profile, the radial profiles of power absorbed by the electrons under the same condition as in Fig. 13 were computed in Fig. 14, by changing the axial position: (a) $z = 10\,\mathrm{cm}$, (b) $z = 20\,\mathrm{cm}$, (c) $z = 30\,\mathrm{cm}$, (d) $z = 40\,\mathrm{cm}$, (e) $z = 50\,\mathrm{cm}$. This power absorption is defined as the scalar product of the electron current density J by the wave electric field E. Here, the main damping mechanism is considered to be collisional damping by electron-neutral particle collision; the ratio of the collision frequency to the wave frequency, ν/ω, of ~ 0.5 was used in the computation. It can be seen from Fig. 14(a) ($z = 10\,\mathrm{cm}$) that the power absorption close to the antenna was mainly limited within the region of the antenna radius ($r < 9\,\mathrm{cm}$), and the peak position was located along the central axis. As z was larger, this position shifted to the outer r position with decreasing the absolute value, and at the line cusp position ($z = 30\,\mathrm{cm}$), the peak power was located in the intermediate region of $r \sim 9\,\mathrm{cm}$ [seen from Figs. 14(b) and 14(c)]. Beyond the cusp position, the peak position shifted back towards the

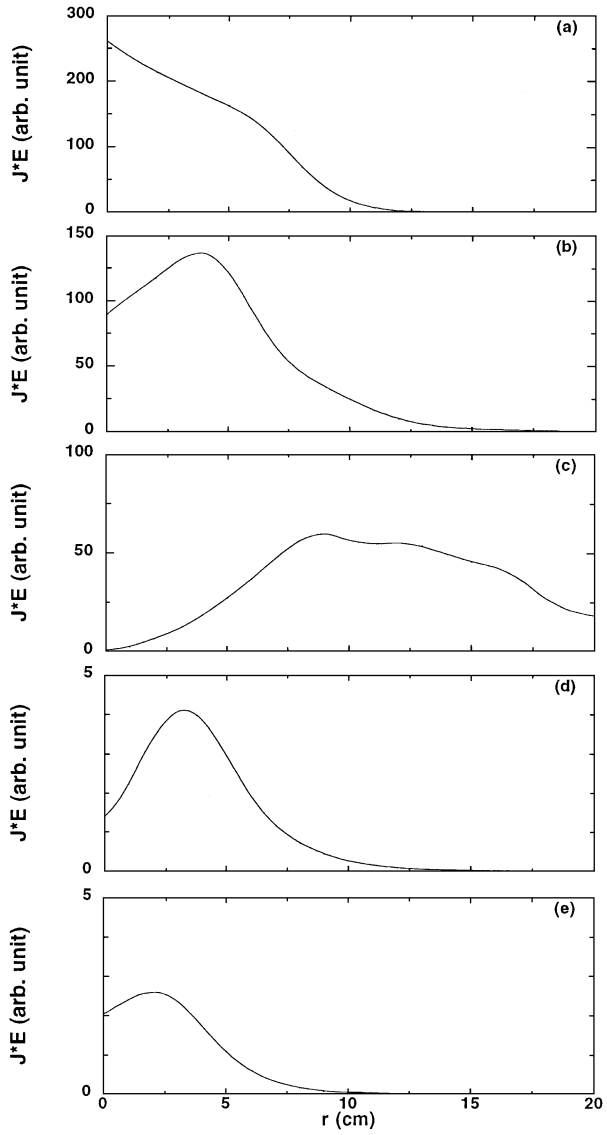

Fig. 14. Radial profiles of $J * E$ by electron with $d = 16\,\mathrm{cm}$ and $I_c = 120\,\mathrm{A}$; (a) $z = 10\,\mathrm{cm}$, (b) $z = 20\,\mathrm{cm}$, (c) $z = 30\,\mathrm{cm}$, (d) $z = 40\,\mathrm{cm}$ (e) $z = 50\,\mathrm{cm}$ (computaion).

center with further decreasing the absolute value [seen from Figs. 14(d) and 14(e)].

For these behaviours of the amplitude and the phase of B_z near the cusp, two qualitative, phenomenological interpretations may be considered as follows. One is that there existed helicon waves with more than one perpendicular wave number:[14] a fundamental radial mode, as well as a higher-order one. Due to interference between the two modes, the calculated dispersion with only the fundamental mode was not in exact agreement with the experimental one. The wave with the higher radial mode (having smaller k_z from the dispersion relation) can penetrate easily across the cutoff layer, compared to the wave with the fundamental radial mode (larger k_z): The transmission coefficients are inversely proportional to the length of the effective cutoff length $2l$ along the axial direction (we did not take into account resonance because of the relatively long wavelength $\sim$ 20 cm just before the cusp), depending on the magnetic field strength and/or the gradient of the field near the cusp position, while proportional to the wavelength.[15] Assuming that the fundamental radial mode $T = 0.38\,\mathrm{cm}^{-1}$ and the second one $T = 0.7\,\mathrm{cm}^{-1}$ ($a = 10$ cm), and the distance l was $\sim$ 5 cm, which corresponded to the axial distance between the position of the critical value $B_c \sim 8$ G and the line cusp position, the coefficient ratio of the second mode to the fundamental one was $\sim$ 5. If the amplitude ratio of the second mode to the fundamental one cannot be neglected before the cusp position, *e.g.*, such as in ref. 14, where this ratio was $\sim$ 0.4, the wave with the second radial mode having larger T and smaller k_z values can be the dominant wave after passing through the cusp position. This can partly explain the discrepancy of the helicon wave dispersion with a fundamental radial mode number after the cusp position (see Fig. 5).

Another interpretation, which may be the dominant mechanism for the wave behavior, is that the helicon wave propagated obliquely to the z axis, i.e., along the field lines near the line cusp position; thereby, the wave was reflected at the chamber wall in the neighborhood of the position, and then the wave beyond the position returned back toward the central region along the field lines (see Figs. 13 and 14). Note that the maximum angle between the direction of the group velocity of the whistler wave and the magnetic field line is less than 20° in the free space.[15] In fact, the radial position having the peak power absorption in Fig. 14 did not deviate from the magnetic field line less than this maximum angle, except for $z < 10$ cm and $z = 30$ cm (line cusp position). In addition, the peak position does not enter the the weak field region, i.e., $B < B_c$, near the line cusp position.

In summary, with the decrease in d, i.e., the decrease in L, the difference in the magnitude B between on axis and off axis increases (see Fig. 2). Therefore, the helicon wave could propagate more obliquely to the z axis with the shorter d (due to larger radial component of the B above the critical value $B_c \sim 8$ G) near the cusp. The discrepancy of the dispersion can be considered as being due to the bending of the magnetic field line and the reflection from the wall region. Note that, to be exact, the ray tracing picture[15] cannot be adopted.

In any case, the excited wave could propagate through the cusp position regarded as an obstacle (effective cutoff region was wider on axis than that at off axis, whose nature depends on I_c and d), with the diffraction just before and the convergence just after the cusp (see Fig. 14), including a possibility for direct tunneling.

5. Conclusion

Characteristics of the RF wave propagation under the cusp magnetic field configurations by changing the coil current I_c and the central distance d between the two coils, i.e., the magnitude and the gradient of the field, were investigated. The spatial profiles of amplitude and phase of the excited magnetic fields in large-diameter plasma were examined by a helicon wave dispersion relation, and were consistent with the computation results obtained from TASK/WF code.

The strong outward damping near the line cusp position is considered to be due to the wave diffraction avoiding the region in the weaker magnetic field, in addition to the wave absorption by the effect of the collisional damping; this wave could propagate further beyond this position when the magnetic field strength B and/or the gradient of the field near the cusp position was larger (L was shorter). The propagating wave before the cusp position was considered as the $m = 0$ mode helicon wave with a fundamental radial mode. For the case of the shorter d, the wave could propagate beyond the cusp position without having the dominant fundamental radial mode of the helicon wave.

Acknowledgment

We would like to thank Professor Y. Kawai for his continuous encouragement.

1) R. W. Boswell: Plasma Phys. Control. Fusion **26** (1984) 1147.
2) F. F. Chen: Plasma Phys. Control. Fusion **33** (1991) 339.
3) S. Shinohara, Y. Miyauchi and Y. Kawai: Plasma Phys. Control. Fusion **37** (1995) 1015.
4) J. Hopwood: Plasma Sources Sci. Technol. **1** (1992) 109.
5) J. Hopwood, C. R. Guarnieri, S. J. Whitehair and J. J. Cuomo: J. Vac. Sci. Technol. A **11** (1993) 147.
6) S. Shinohara, S. Takechi and Y. Kawai: Jpn. J. Appl. Phys. **35** (1996) 4503.
7) S. Shinohara, S. Takechi, N. Kaneda and Y. Kawai: Plasma Phys. Control. Fusion **39** (1997) 1479.
8) S. Takechi, S. Shinohara and Y. Kawai: Jpn. J. Appl. Phys. **36** (1997) 4558.
9) S. Takechi, S. Shinohara and Y. Kawai: Surf. Coat. Technol. **112** (1999) 15.
10) S. Takechi and S. Shinohara: Proc. 4th Int. Conf. Reactive Plasmas and 16th Symp. Plasma Processing (Hawaii, 1998) p. 153.
11) S. Shinohara and Y. Kawai: Jpn. J. Appl. Phys. **34** (1995) L1571.
12) A. Fukuyama and Y. Ichida: Proc. Int. Conf. Plasma Physics (Nagoya, 1996) Vol. 2, p. 1342.
13) V. A. Godyak and R. B. Piejak: J. Appl. Phys. **82** (1997) 5944.
14) Y. Sakawa, N. Koshikawa and T. Shoji: Plasma Sources Sci. Technol. **6** (1997) 96.
15) T. H. Stix: *Waves in Plasmas* (AIP, New York, 1992).